STRUCTURAL BIOLOGY COMMUNICATIONS

ISSN 2053-230X

Crystal structure of carbon–nitrogen hydrolase from *Helicobacter pylori* G27

Aruesha Srivastava,[a] Jesuferanmi P. Ayanlade,[b] Lema Suleiman,[c] Hannah Udell,[d,e] Jan Abendroth,[d,f] Donald J. Lorimer,[d,f] Thomas E. Edwards,[d,f] Bart L. Staker,[d,e] Rachael Zigweid,[d,e] Sandhya Subramanian,[d,e] Peter J. Myler,[d,e,g] Graham Chakafana[h]* and Oluwatoyin A. Asojo[d,i,j]*

[a]California Institute of Technology, 1200 East California Boulevard, Pasadena, CA 91125, USA, [b]School of Arts and Sciences, Dartmouth College, Hanover, New Hampshire, USA, [c]College of William and Mary, Williamsburg, Virginia, USA, [d]Seattle Structural Genomics Center for Infectious Diseases, Seattle, Washington, USA, [e]Center for Global Infectious Disease Research, Seattle Children's Research Institute, 1916 Boren Avenue, Seattle, WA 98101, USA, [f]UCB Biosciences, Bainbridge Island, WA 98110, USA, [g]Departments of Pediatrics, Biomedical Informatics, Medical Education and Global Health, University of Washington, Seattle, WA 98185, USA, [h]Chemistry and Biochemistry, Hampton University, Hampton, VA 23666, USA, [i]Dartmouth Cancer Center, One Medical Center Drive, Lebanon, NH 03756, USA, and [j]Biochemistry and Cell Biology, Dartmouth Geisel School of Medicine, Lebanon, NH 03756, USA. *Correspondence e-mail: graham.chakafana@hamptonu.edu, oluwatoyin.a.asojo@dartmouth.edu

Received 6 January 2026
Accepted 6 February 2026

Edited by J. Agirre, University of York, United Kingdom

This article is part of a special issue celebrating early career researchers in structural science.

Keywords: *Helicobacter pylori*; carbon–nitrogen hydrolases; SSGCID; structural genomics; hydrolases.

PDB reference: carbon–nitrogen hydrolase from *Helicobacter pylori* G27, 6mg6

Supporting information: this article has supporting information at journals.iucr.org/f

Carbon–nitrogen hydrolases (CNHs) are members of the diverse nitrilase superfamily of enzymes that facilitate cellular adaptation to environmental stress by metabolizing nitrogen, detoxifying xenobiotics and catabolizing environmentally derived metabolites. *Helicobacter pylori* CNH (*Hp*CNH) may contribute to metabolic flexibility under acid stress, detoxification of reactive nitrogen species or nutrient scavenging in the nutrient-limited gastric environment. Here, we report the 2.1 Å resolution crystal structure of a CNH from *H. pylori* strain G27 (PDB entry 6mg6). *Hp*CNH adopts the characteristic nitrilase-superfamily $\alpha\beta\beta\alpha$-sandwich core and contains the conserved catalytic cysteine typical of enzymatically active CNHs. The overall structure and active site of *Hp*CNH are most similar to those of carbamoylputrescine amidohydrolase from the plant *Medicago truncatula*. Despite structural variations in loop regions, including near the active site, *Hp*CNH retains the key residues required to bind putrescine and the prototypical *N*-carbamoylputrescine amidase active site.

1. Introduction

Helicobacter pylori is a Gram-negative, microaerophilic bacterium that colonizes the human gastric mucosa and infects more than half of the global population (Warren & Marshall, 1983; Malfertheiner *et al.*, 2023; Moss *et al.*, 2023). Persistent *H. pylori* infection is the primary cause of chronic gastritis, peptic ulcer disease and gastric adenocarcinoma, and the World Health Organization classifies *H. pylori* as a group 1 carcinogen (Malfertheiner *et al.*, 2023; Moss *et al.*, 2023; Cover & Blaser, 2009). *H. pylori* persists in the gastric mucosa by modulating environmental conditions and host responses using mechanisms including hydrolysis of urea to buffer acidic pH, modulation of gene expression in response to acid stress and alteration of gastric epithelial biology (Benoit *et al.*, 2020; Kuhns *et al.*, 2016; Warren & Marshall, 1983; Malfertheiner *et al.*, 2023; Moss *et al.*, 2023).

Structure–function studies of *H. pylori* proteins, including carbon–nitrogen hydrolases (CNHs), at the Seattle Structural Genomics Center for Infectious Disease (SSGCID) are under way to generate insights into the structural basis of *H. pylori* survival mechanisms. This is because CNHs facilitate cellular

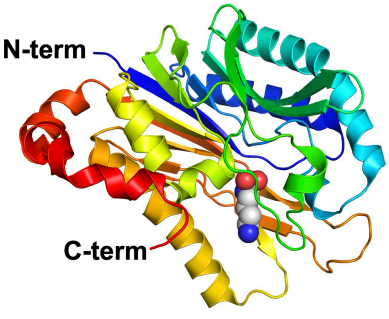

adaptation to environmental stress by metabolizing nitrogen, detoxifying xenobiotics and catabolizing environmentally derived metabolites (Bork & Koonin, 1994). CNHs hydrolyze nonpeptide C—N bonds in substrates such as amides, nitriles, carbamates and urea, and are widely distributed across bacteria, archaea and plants (Bork & Koonin, 1994). Many bacterial CNHs, including *H. pylori* CNH (*Hp*CNH), remain poorly characterized, and structural characterization is essential to infer biochemical function, substrate specificity and potential physiological roles.

*Hp*CNH is annotated as an *N*-carbamoylputrescine amidase, placing it within the putrescine biosynthetic process from arginine, a pathway critical for polyamine metabolism. Polyamines such as putrescine play key roles in cell proliferation, biofilm formation and acid resistance in many bacterial species, making this enzyme a potential player in the adaptation of *H. pylori* to gastric acidity and stress (Nair *et al.*, 2025; Sagar *et al.*, 2021). We present the recombinant production and crystal structure of *Hp*CNH as part of efforts to clarify its functions.

2. Materials and methods

2.1. Macromolecule production

*Hp*CNH was cloned, expressed and purified using standard protocols established at the SSGCID (Stacy *et al.*, 2011; Serbzhinskiy *et al.*, 2015; Rodríguez-Hernández *et al.*, 2023). Briefly, the full-length gene for carbon–nitrogen hydrolase from *H. pylori* G27 (UniProt B5Z8D8) encoding amino acids 1–292 was PCR-amplified from genomic DNA using the primers shown in Table 1. The gene was cloned into the expression vector BG1861 encoding an N-terminal His-tag to generate plasmid DNA, which was transformed into chemically competent *Escherichia coli* BL21(DE3)R3 Rosetta cells. The plasmid containing His-*Hp*CNH was tested for expression, and 2 l of culture was grown using auto-induction medium (Studier, 2005) in a LEX Bioreactor (Epiphyte Three) as described previously (Serbzhinskiy *et al.*, 2015). Glycerol stocks of the expression clone may be requested at https://www.ssgcid.org/available-materials/expression-clones/.

*Hp*CNH was purified using the previously described SSGCID two-step protocol of an immobilized metal (Ni^{2+}) affinity chromatography (IMAC) step followed by size-exclusion chromatography (SEC) on an ÄKTApurifier 10 (GE Healthcare) using automated IMAC and SEC programs (Serbzhinskiy *et al.*, 2015). Briefly, thawed bacterial pellets (∼25 g) were lysed by sonication in 200 ml lysis buffer [20 m*M* HEPES pH 7.0, 300 m*M* NaCl, 5%(*v*/*v*) glycerol, 0.5%(*w*/*v*) CHAPS, 30 m*M* imidazole, 21 m*M* $MgCl_2$, 1 m*M* TCEP and five protease-inhibitor cocktail tablets (cOmplete Mini, EDTA-free, Roche, Basel, Switzerland)]. The solution was incubated with 20 µl Benzonase nuclease (EMD Chemicals, Gibbstown, New Jersey, USA) for 40 min at room temperature under gentle agitation. The lysate was centrifuged with a Sorvall RC5 at 10 000 rev min^{-1} for 60 min at 4°C in an F14S Rotor (Thermo Fisher, Waltham, Massachusetts, USA). The clarified lysate was filtered through a 0.45 µm cellulose acetate filter (Corning Life Sciences, Lowell, Massachusetts, USA). The IMAC step used a HisTrap FF 5 ml column (GE Biosciences, Piscataway, New Jersey, USA) equilibrated in binding buffer [20 m*M* HEPES pH 7.0, 300 m*M* NaCl, 5%(*v*/*v*) glycerol, 30 m*M* imidazole] and eluted over a 7 column-volume linear gradient with elution buffer [20 m*M* HEPES pH 7.0, 300 m*M* NaCl, 5%(*v*/*v*) glycerol, 500 m*M* imidazole]. IMAC peak fractions were pooled and concentrated to 5 ml using an Amicon Ultra centrifugal filter (Millipore, Billerica, Massachusetts, USA). The SEC step used a Superdex 75 26/60 column (GE Biosciences) equilibrated in SEC buffer [20 m*M* HEPES pH 7.0, 300 m*M* NaCl, 5%(*v*/*v*) glycerol, 1 m*M* TCEP] attached to an ÄKTAprime plus FPLC system (GE Biosciences). 100 ml SEC buffer was run over the column, and peak fractions were collected at 1.5 ml min^{-1} for an additional 180 ml. Peak fractions were collected and assessed by SDS–PAGE on a 4–20% protein gel (Invitrogen) and visualized by Coomassie staining with InstantBlue colloidal stain (Expedeon, San Diego, California, USA). *Hp*CNH eluted from SEC as a single monodisperse peak of ∼90 kDa (based on molecular-weight standards), suggesting the formation of the assigned dimer by the *Protein Interfaces, Surfaces and Assemblies* (*PISA*) service at the European Bioinformatics Institute (https://www.ebi.ac.uk/pdbe/prot_int/pistart.html). SEC peak fractions were pooled, concentrated to ∼20 mg ml^{-1}, flash-frozen in liquid nitrogen and stored at −80°C. Recombinant *Hp*CNH protein is available for request online at https://www.ssgcid.org/available-materials/ssgcid-proteins/.

Table 1
Macromolecule-production information.

Source organism	*Helicobacter pylori* (strain G27)
DNA source	Nina Salama, FHCRC
Forward primer	5′-CTCACCACCACCACCATATGATT TATGCAGGCGTCCTCCA-3′
Reverse primer	5′-ATCCTATCTTACTCACTTAAATATAG CGTTTCAACAAATCGTTATA-3′
Expression vector	BG1861
Expression host	*Escherichia coli* BL21(DE3) Rosetta
Complete amino-acid sequence of the construct produced	**MAHHHHHH**MIYAGVLQHAYCGSRKKTIE HTANLLEQALKKHPKTNLVVLQELNPY SYFCQSENPKFFDLGEYFEEDKAFFSA LAQKFQVVLIASLFEKRAKGLYHNSAV VFEKDGSIAGVYRKMHIPDDPGFYEKF YFTPGDLGFEPIITSVGKLGLMVCWDQ WYPEAARIMALKGAEILIYPSAIGFLE EDSNEEKKRQQNAWETIQRGHAIANGL PLIATNRVGVELDPSGAIKGGITFFGS SFVVGALGEFLAKASDKEEILYAEIDL ERTEEVRRMWPFLRDRRIDFYNDLLKR YI

2.2. Crystallization

*Hp*CNH crystallized at 290 K using sitting-drop vapor diffusion directly from Microlytic MCSG1 screen condition G8 (Table 2). Briefly, equal volumes of 19.9 mg ml^{-1} *Hp*CNH and 25%(*w*/*v*) PEG 3350, 200 m*M* ammonium sulfate, 100 m*M* Tris–HCl pH 8.5 were mixed in sitting-drop screens (Table 2). Before data collection, the crystals were harvested and cryoprotected with 15%(*v*/*v*) ethylene glycol (Table 2).

Table 2
Crystallization.

Method	Vapor diffusion, sitting drop
Plate type	96-well plates, SwissSci MRC2 tray
Temperature (K)	290
Protein concentration (mg ml^{-1})	19.9
Buffer composition of protein solution	20 m*M* HEPES pH 7.0, 300 m*M* NaCl, 5%(*v*/*v*) glycerol, 1 m*M* TCEP
Composition of reservoir solution	25%(*w*/*v*) PEG 3350, 200 m*M* ammonium sulfate, 100 m*M* Tris–HCl pH 8.5
Volume and ratio of drop	0.4 µl:0.4 µl
Volume of reservoir (µl)	80
Composition of cryoprotectant solution	21.25%(*w*/*v*) PEG 3350, 170 m*M* ammonium sulfate, 85 m*M* Tris–HCl pH 8.5, 15% ethylene glycol

Table 3
Data collection and processing.

Values in parentheses are for the outer shell.

Diffraction source	ALS beamline 5.0.1
Wavelength (Å)	0.97741
Temperature (K)	100
Detector	Dectris PILATUS3 6M
Space group	$P2_12_12$
a, *b*, *c* (Å)	137.58, 91.38, 95.04
α, β, γ (°)	90, 90, 90
Resolution range (Å)	47.58–2.10 (2.15–2.10)
Completeness (%)	99.400 (100.000)
Multiplicity	6.543 (6.670)
$\langle I/\sigma(I)\rangle$	25.59 (2.0)
$R_{\rm r.i.m.}$	0.042 (0.589)
Overall *B* factor from Wilson plot (Å^2)	50.3

Table 4
Structure refinement.

Values in parentheses are for the outer shell.

Resolution range (Å)	47.58–2.10 (2.15–2.10)
Completeness (%)	99.4 (99.0)
No. of reflections, working set	70175 (4496)
No. of reflections, test set	2044 (161)
Final $R_{\rm cryst}$	0.168 (0.219)
Final $R_{\rm free}$	0.208 (0.251)
No. of non-H atoms	
Protein	9123
Ion	5
Water	393
Total	9521
R.m.s. deviations	
Bond lengths (Å)	0.007
Angles (°)	0.845
Average *B* factors (Å^2)	
Protein	56.3
Ion	83.1
Water	50.2
Ramachandran plot	
Most favored (%)	98.3
Allowed (%)	2.6
Outliers (%)	0.09

2.3. Data collection and processing

Data were collected at 100 K on Advanced Light Source (ALS) beamline 5.0.1 at Lawrence Berkeley National Laboratory (Table 3). Data were integrated with *XDS* and reduced with *XSCALE* (Kabsch, 2010). Raw X-ray diffraction images are stored at the Integrated Resource for Reproducibility in Macromolecular Crystallography at https://www.proteindiffraction.org.

2.4. Structure solution and refinement

The structure of *Hp*CNH was determined by molecular replacement with *Phaser* (McCoy *et al.*, 2007) from the *CCP*4 suite of programs (Collaborative Computational Project, Number 4, 1994; Krissinel *et al.*, 2004; Winn *et al.*, 2011; Agirre *et al.*, 2023) using PDB entry 5h8i (Sekula *et al.*, 2016) as the search model. The structure was refined using iterative cycles of *Phenix* (Adams *et al.*, 2011) followed by manual rebuilding of the structure using *Coot* (Emsley & Cowtan, 2004; Emsley *et al.*, 2010). The structure quality was checked using *MolProbity* (Williams *et al.*, 2018). Data-reduction and refinement statistics are shown in Table 4. The coordinates and structure factors have been deposited in the Worldwide PDB (wwPDB) as entry 6mg6.

3. Results and discussion

*Hp*CNH crystallized in the orthorhombic space group $P2_12_12$, and the crystal structure was refined at 2.10 Å resolution with an $R_{\rm work}$ of 0.168 and an $R_{\rm free}$ of 0.208 (Tables 3 and 4). The final high-quality model has well defined electron density (Fig. 1*a*). The asymmetric unit contains four copies of the polypeptide (chains *A*–*D*), forming a dimer of two tightly packed dimers (Fig. 1*b*). Each chain forms a prototypical four-layered $\alpha\beta\beta\alpha$ nitrilase structure, with three β-sheets (Fig. 1*c*). The 294 amino acids of each chain fold with secondary-structure topology of 27.2% β-strand, 27.2% α-helix, 7.8% 3_{10}-helix and 37.8% other (mostly flexible loop regions). Each *Hp*CNH chain contains three sheets (two six-stranded mixed sheets and one three-stranded antiparallel sheet), five β-hairpins, five β-bulges, 15 strands, 12 helices, 29 helix–helix interactions, 15 β-turns and four γ-turns. Further topological details from *PDBsum* are given in Supplementary Scheme S1. Pairwise *PDBeFold* superpositions reveal that the four copies are very similar, with an r.m.s.d. of 0.15–0.40 Å over all main-chain atoms. The four polypeptide chains exhibit minimal conformational heterogeneity at the termini and surface-exposed loops (Fig. 1*d*).

*Hp*CNH is predicted to be a biological dimer based on *PISA* analysis (Krissinel, 2015) and agreement with SEC data (Supplementary Fig. S1). There are two *Hp*CNH dimers in the asymmetric unit. Each has a large, buried surface area (Fig. 1*b*, Table 5). There are 50 interface amino acids per monomer, eight salt bridges, 39 hydrogen bonds and 375 nonbonded contacts at the dimer interface. Both dimers are consistent

Table 5
The *Hp*CNH structure contains two prototypical CNH dimers per asymmetric unit of the complex.

	*Hp*CNH (chains *A*:*B*)	*Hp*CNH (chains *C*:*D*)
Multimeric state	Homodimer	Homodimer
Total solvent-accessible surface area of the complex (Å^2)	20679	20621
Buried surface area (Å^2)	5584	4746
Dissociation area (Å^2)	2111	2373
Dissociation energy (ΔG_{diss}) (kcal mol^{-1})	31.83	30.17
Dissociation entropy ($T\Delta S_{diss}$) (kcal mol^{-1})	13.85	13.67
No. of interfaces	1	1

with biologically relevant dimers observed in other nitrilases (Bork & Koonin, 1994; Nair *et al.*, 2025; Sagar *et al.*, 2021; Sekula *et al.*, 2016).

ENDScript (Gouet *et al.*, 2003; Robert & Gouet, 2014) analysis revealed the most similar crystal structure to *Hp*CNH to be that of the molecular-replacement search model, *M. truncatula* carbamoylputrescine amidohydrolase (*Mtr*CPA) in complex with *N*-(dihydroxymethyl)putrescine (PDB entry 5h8i), followed by the C158S mutant of the same protein, PDB entry 5h8k (Sekula *et al.*, 2016). *Mtr*CPA shares ∼41% sequence identity with *Hp*CNH, as well as an r.m.s.d. of ∼1.4 Å of C_α atoms per protomer. A *BlastP* search against the

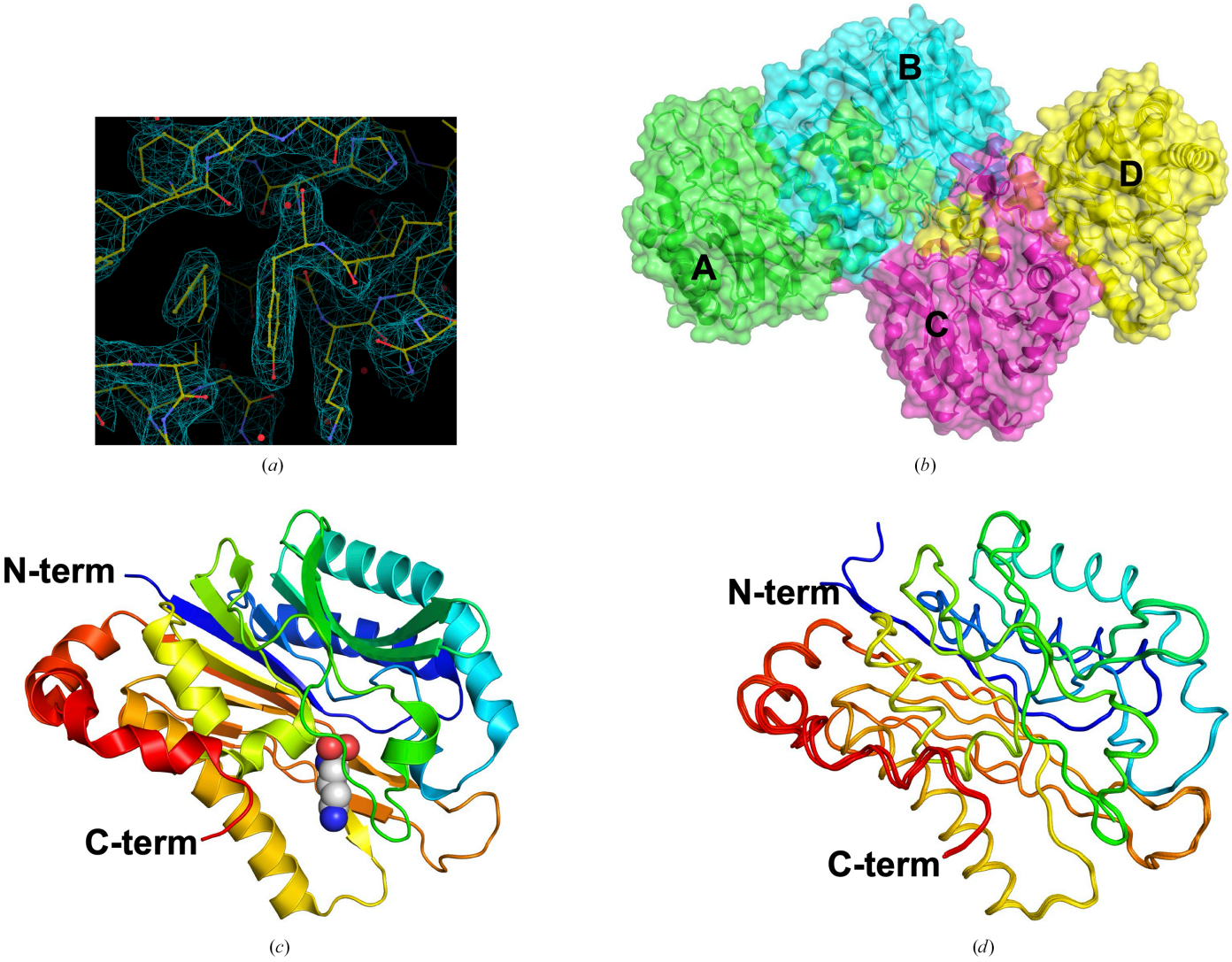

(*a*) (*b*) (*c*) (*d*)

Figure 1
Overall structure of *Hp*CNH. (*a*) The refined model fits well into the 1.2σ 2$F_o - F_c$ electron-density map (blue mesh). (*b*) *Hp*CNH has four protomers in the asymmetric unit, and they are comprised of two tightly packed prototypical CNH dimers, indicated by dimer *AB* and dimer *CD*. (*c*) A cartoon, colored in a rainbow from red at the C-terminus to blue at the N-terminus, of a representative *Hp*CNH protomer reveals the canonical nitrilase fold. The predicted active site is indicated with a molecule of putrescine in a space-filling model based on the structure of *Mtr*CPA (PDB entry 5h8i). (*d*) A ribbon diagram of superposed protomers, colored in a rainbow from blue at the N-terminus to red at the C-terminus, reveals nearly identical structures.

PDB reveals it to be the only protein within the PDB that shares over 34% sequence identity with *Hp*CNH. *Mtr*CPA catalyzes the final step of putrescine biosynthesis: the hydrolysis of carbamoylputrescine to putrescine. The closest structure after *Mtr*CPA is that of mouse nitrilase: PDB entry 2w1v (Barglow *et al.*, 2008). The subsequent closest structures are of complexes of the C146A mutant of the amidase from *Pyrococcus horikoshii*: PDB entries 7ovg and 6ypa (Makumire *et al.*, 2022). The structure of β-alanine synthase from *Drosophila melanogaster*, PDB entry 2vhh (Lundgren *et al.*, 2008), is more similar to *Hp*CNH than the wild-type amidase from *P. horikoshii*, PDB entry 1j31 (Sakai *et al.*, 2004). The remaining similar structures are PDB entries 3ivz, 8pt4, 1ems, 6ftq, 2ggk, 1fo6, 2ggl, 1erz, 8hpc, 1uf4, 7elf, 4hg3, 3hkx, 4izt,

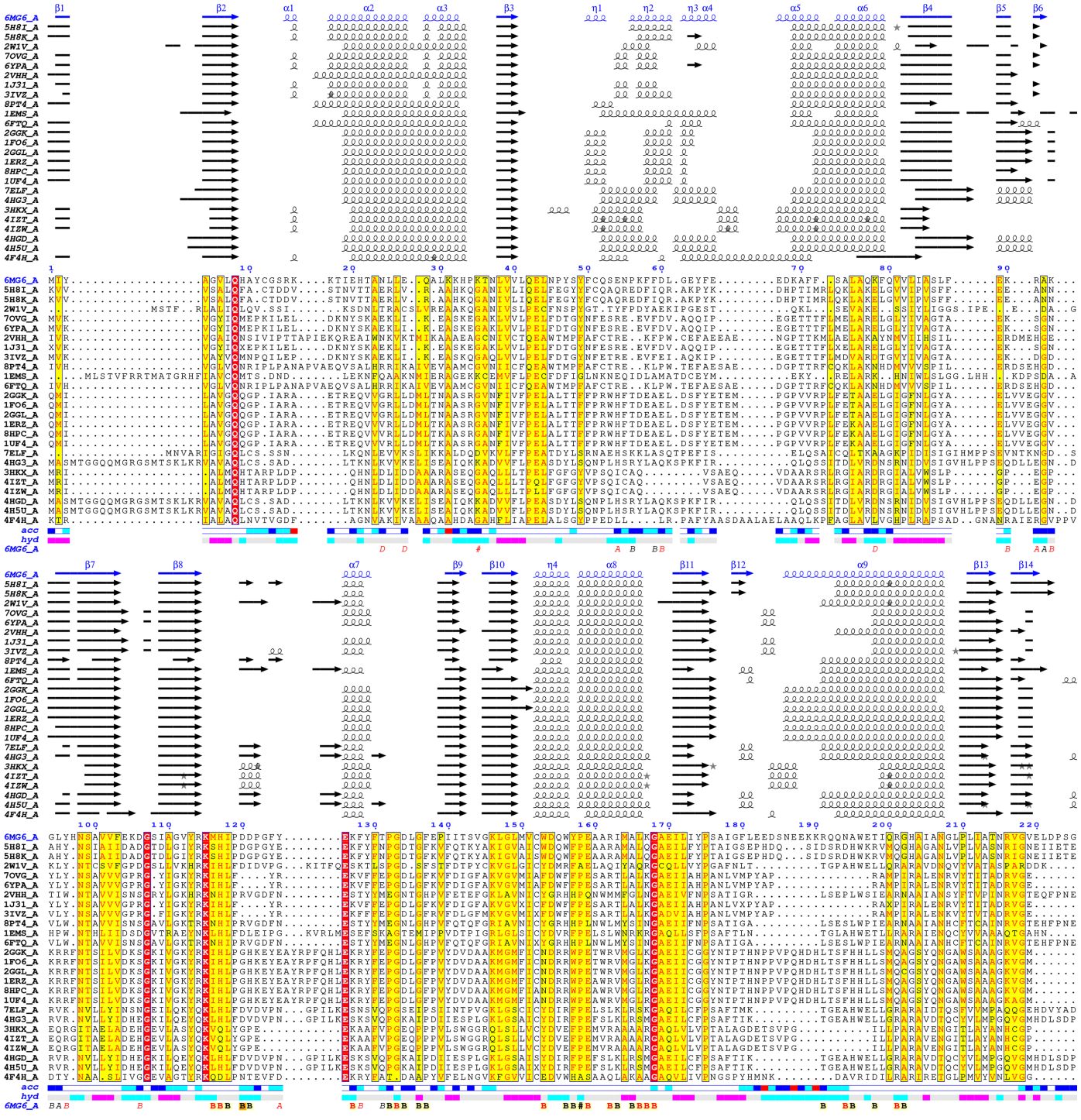

Figure 2
ENDScript analysis reveals the nearest structural neighbors of *Hp*CNH. Identical and conserved residues are highlighted in red and yellow, respectively. The different secondary-structure elements shown are α-helices (α), 3_{10}-helices (η), β-strands (β) and β-turns (TT) (Gouet *et al.*, 1999, 2003).

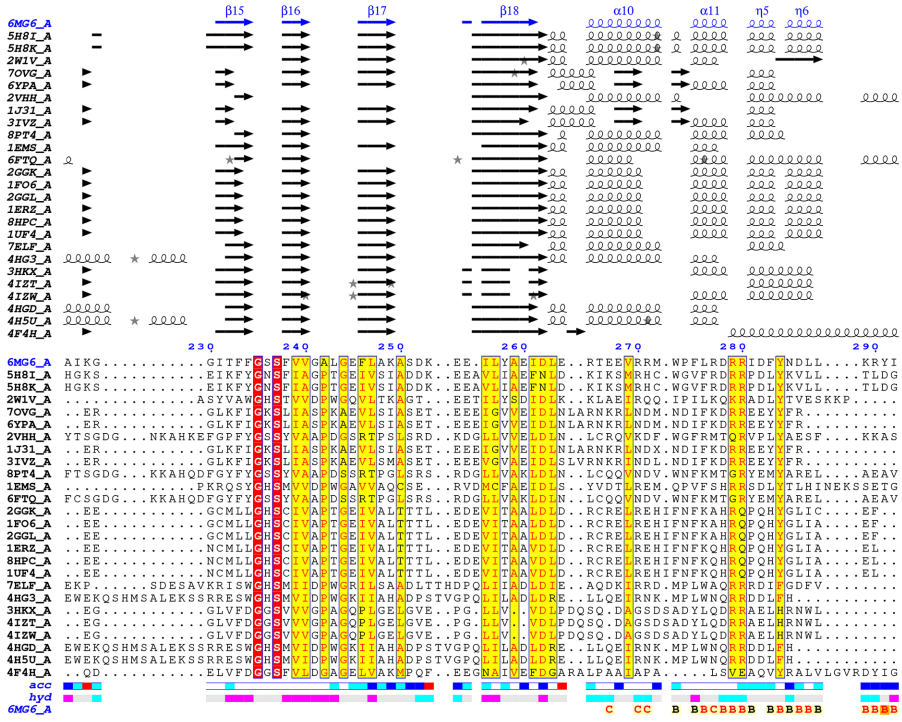

Figure 2 (continued)

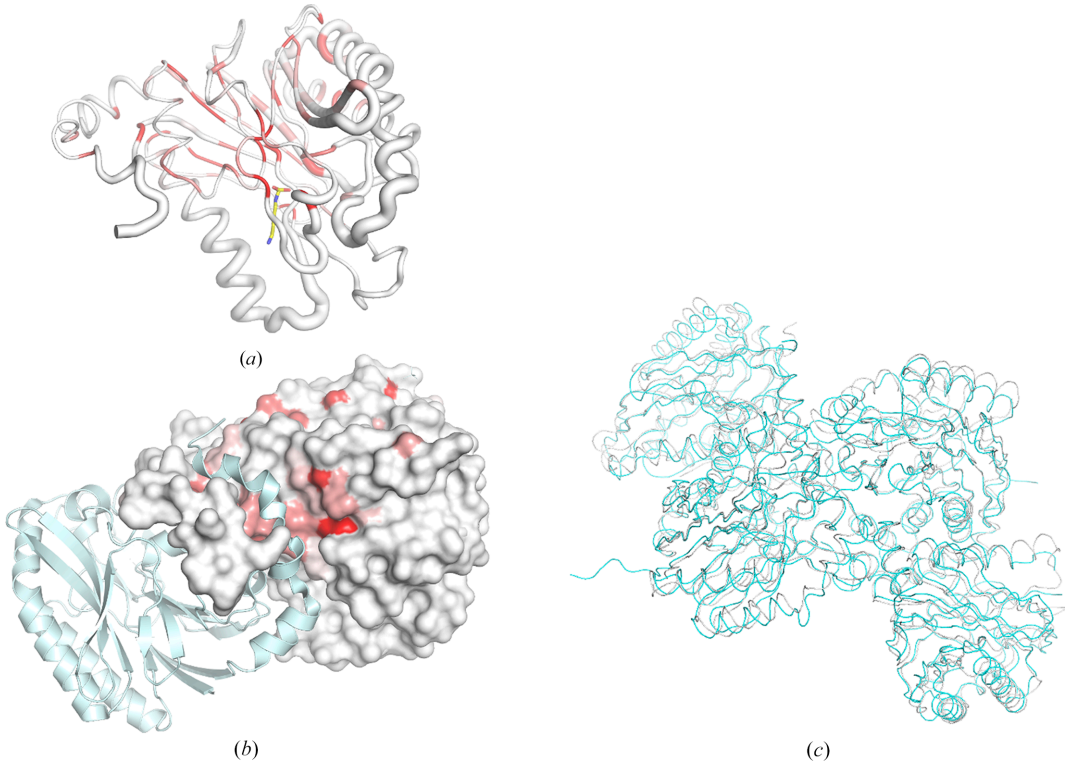

Figure 3
Comparison of *Hp*CNH with its closest structural neighbors. (*a*) Sausage plot generated by *ENDScript*. The ribbon (sausage) shows relative secondary-structural conservation compared with other nitrilase structures. The ribbon thickness reflects the level of secondary-structure similarity, with thinner ribbons indicating more conserved regions and thicker ribbons suggesting lower conservation, as determined by r.m.s.d. alignment of structures shown in Fig. 2. The ribbon is colored based on sequence conservation, with red indicating identical residues. Also included is putrescine from PDB entry 5h8i, shown as yellow sticks. (*b*) *Hp*CNH forms a typical nitrilase homodimer, with interaction between monomers involved in the catalytic cavity. One protomer is depicted as a surface plot, while the other is shown as a cyan cartoon. The protomer represented in the surface plot in (*b*) is in the same orientation as the protomer in (*a*). The surface plot is colored by sequence conservation, with red indicating identical residues. (*c*) Ribbon diagram of superposed tetramers of *Hp*CNH (PDB entry 6mg6, gray) and *Mtr*CPA (PDB entry 5h8i, cyan) reveals a similar overall quaternary structure.

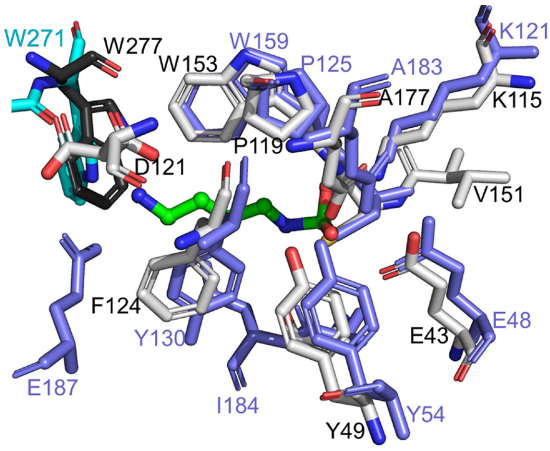

(*a*)

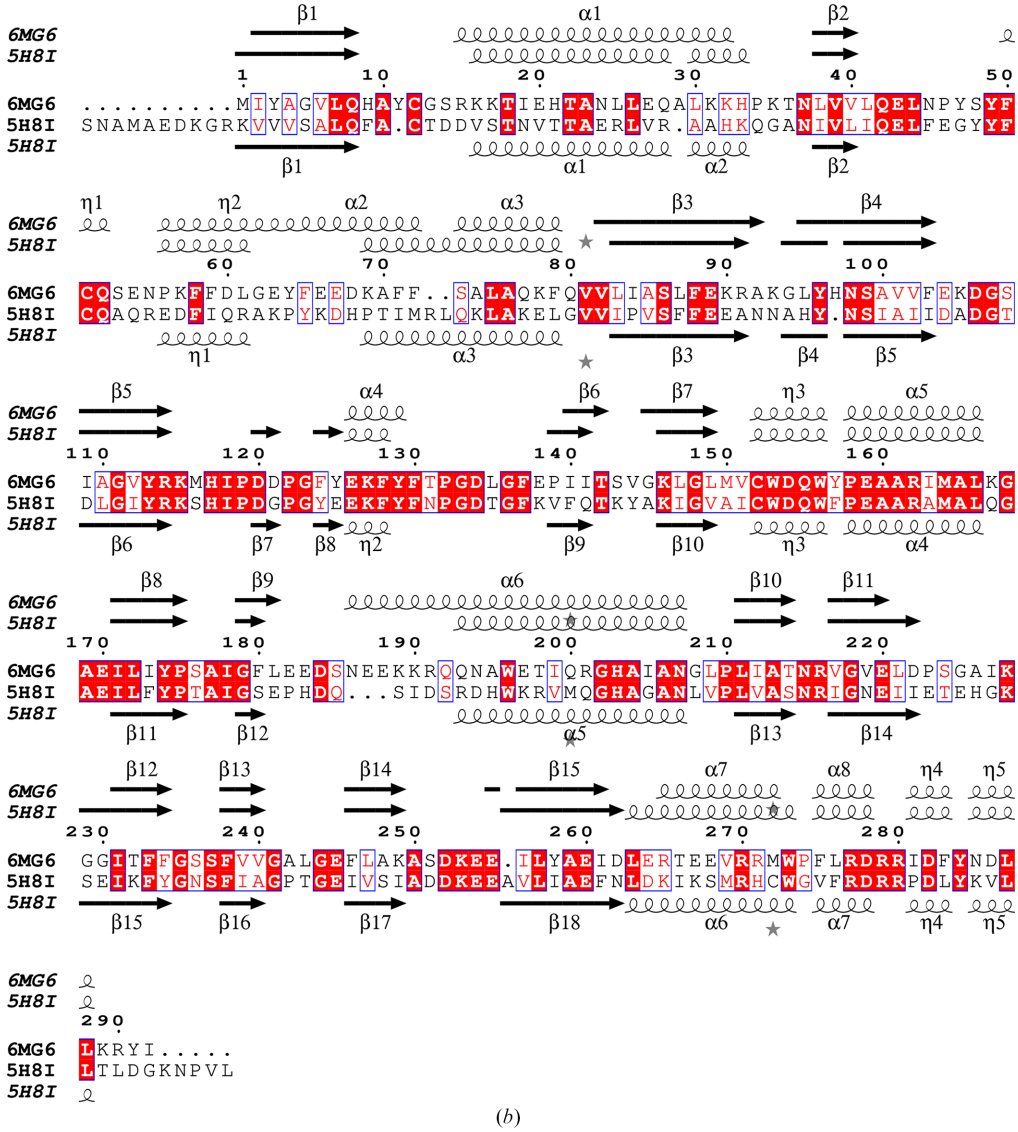

(*b*)

Figure 4
Comparison of *Hp*CNH with *Mtr*CPA reveals conserved putrescine-binding residues. (*a*) The putrescine (green sticks) binding-cavity residues of both the *Hp*CNH (gray sticks) and *Mtr*CPA (blue sticks) structures are conserved. Also shown are residues from across the dimer interface of *Hp*CNH (cyan sticks) and *Mtr*CPA (black sticks). (*b*) Structure-based sequence alignment of *Hp*CNH (PDB entry 6mg6) and *Mtr*CPA (PDB entry 5h8i) structures. The secondary-structure elements are as follows: α-helices are shown as large coils, 3_{10}-helices are shown as small coils labeled η, β-strands are shown as arrows labeled β and β-turns are labeled TT. The identical residues are shown in white font on a red background, conserved residues are shown in red font and conserved regions are shown in blue boxes. (*b*) was generated using *ESPript* 3.0 (Gouet *et al.*, 1999, 2003).

4izw, 4hgd, 4h5u and 4f4h (Raczynska *et al.*, 2011; Cederfelt *et al.*, 2023; Pace *et al.*, 2000; Maurer *et al.*, 2018; Chiu *et al.*, 2006; Wang *et al.*, 2001; Jin *et al.*, 2021; Liu *et al.*, 2013; Nel *et al.*, 2011). None of these similar structures are of *H. pylori* proteins. *ENDScript* also reveals close alignment of core secondary-structure elements, while highlighting variations in surface loops and peripheral regions (Fig. 2). Conserved residues are shown in red, except for the catalytic cysteine, because the structures include mutant proteins where the cysteine has been changed to various amino acids or is covalently bound to a ligand (Fig. 2). An *ENDScript*-generated sausage plot reveals that *Hp*CNH conserves the $\alpha\beta\beta\alpha$ core of other nitrilases (Fig. 3*a*). The least conserved regions identified by *ENDScript* alignment are in the loop regions (Fig. 2).

The sausage plot reveals that the core strands exhibit the highest levels of both structural and sequence conservation (Fig. 3*a*). *PDBeFold* analysis (https://www.ebi.ac.uk/msd-srv/ssm) with the default threshold cutoff of 70% identified similar results as *ENDScript* (Supplementary Table S1). Notably, the closest structures to *Hp*CNH were of carbamoylputrescine amidohydrolase (CPA) from the model legume plant *M. truncatula* (Sekula *et al.*, 2016). Interestingly, the *Hp*CNH tetramer and the *Mtr*CPA tetramer align with an r.m.s.d. of ∼1.5 Å for all main-chain tetramer C_α atoms, revealing a conserved quaternary structure (Fig. 3*c*). This is comparable to the r.m.s.d. of ∼1.4 Å for all main-chain protomer C_α atoms. Thus, we can conclude that *Hp*CNH and *Mtr*CPA have similar tertiary and quaternary structures.

Although no biologically relevant compounds were soaked or co-crystallized with the *Hp*CNH structure, comparison of the putative active site with that of the ternary complex of *Mtr*CPA with (dihydroxymethyl)putrescine (PDB entry 5h8i) reveals an active site containing the catalytic cysteine and several other residues required for amidase activity (Fig. 4*a*). Residues that are identically conserved from *Mtr*CPA are Cys158, Pro128, Trp159, Glu48, Ala183, Tyr54 and Lys121, which in *Hp*CNH correspond to Cys152, Pro119, Trp153, Glu43, Ala177, Tyr49 and Lys115, respectively (Fig. 4*b*). Similar residues in the active site also help to retain charge and interactions. For example, *Hp*CNH contains Phe124, whereas *Mtr*CPA contains Tyr130. A second example is Glu187 in *Mtr*CPA, which is from a loop that is missing in *Hp*CNH. Instead, Asp121 from another loop in *Hp*CNH is positioned similarly and may interact with ligands in the binding cavity in its place. Additionally, Trp277 in *Mtr*CPA, which interacts with ligands across the dimer interface, aligns with Trp271 in HpCNH, as does the helix containing it (Figs. 4*a* and 4*b*).

The structure of *Hp*CNH reveals conserved residues that are required to bind putrescine comparably to *Mtr*CPA. Overall, *Hp*CNH has conserved secondary-structure elements typical of CNHs, with variable loops in proximity to the active site (Fig. 3*a*). *Hp*CNH has the necessary active-site residues required to function as an *N*-carbamoylputrescine amidase. Future studies will include determination of the *N*-carbamoylputrescine amidohydrolase activity of *Hp*CNH using established methods (Piotrowski *et al.*, 2003). These methods will also be used to determine whether *Hp*CNH is inhibited by known *Mtr*CPA inhibitors. Once activity and inhibition are confirmed, co-crystallization with putrescine and selected inhibitors will be conducted.

4. Conclusion

The structure of *Hp*CNH retains the conserved primary- and secondary-structure elements typical of CNHs, with variable loops in proximity to the active site. While *Hp*CNH retains the catalytic site residues required to function as an *N*-carbamoylputrescine amidase, structure–function activity studies are required to determine the *N*-carbamoylputrescine amidase activity and establish *Hp*CNH as a target for structure-based drug discovery.

Acknowledgements

This project is part of a continuing SSGCID collaboration that trains undergraduate students in structural science, rational structure-based drug discovery and scientific communication. AS, JPA and LS are undergraduate students mentored by OAA.

Funding information

This project has been funded in whole or in part with Federal funds from the National Institute of Allergy and Infectious Diseases, National Institutes of Health, Department of Health and Human Services under Contract No. 75N93022C00036. This research used resources of the Advanced Light Source, a US DOE Office of Science User Facility under contract No. DE-AC02-05CH11231. We are also grateful for access to Dartmouth Cancer Center resources supported by NCI P30CA023108 and philanthropy.

References

Adams, P. D., Afonine, P. V., Bunkóczi, G., Chen, V. B., Echols, N., Headd, J. J., Hung, L. W., Jain, S., Kapral, G. J., Grosse Kunstleve, R. W., McCoy, A. J., Moriarty, N. W., Oeffner, R. D., Read, R. J., Richardson, D. C., Richardson, J. S., Terwilliger, T. C. & Zwart, P. H. (2011). *Methods*, **55**, 94–106.

Agirre, J., Atanasova, M., Bagdonas, H., Ballard, C. B., Baslé, A., Beilsten-Edmands, J., Borges, R. J., Brown, D. G., Burgos-Mármol, J. J., Berrisford, J. M., Bond, P. S., Caballero, I., Catapano, L., Chojnowski, G., Cook, A. G., Cowtan, K. D., Croll, T. I., Debreczeni, J. É., Devenish, N. E., Dodson, E. J., Drevon, T. R., Emsley, P., Evans, G., Evans, P. R., Fando, M., Foadi, J., Fuentes-Montero, L., Garman, E. F., Gerstel, M., Gildea, R. J., Hatti, K., Hekkelman, M. L., Heuser, P., Hoh, S. W., Hough, M. A., Jenkins, H. T., Jiménez, E., Joosten, R. P., Keegan, R. M., Keep, N., Krissinel, E. B., Kolenko, P., Kovalevskiy, O., Lamzin, V. S., Lawson, D. M., Lebedev, A. A., Leslie, A. G. W., Lohkamp, B., Long, F., Malý, M., McCoy, A. J., McNicholas, S. J., Medina, A., Millán, C., Murray, J. W., Murshudov, G. N., Nicholls, R. A., Noble, M. E. M., Oeffner, R., Pannu, N. S., Parkhurst, J. M., Pearce, N., Pereira, J., Perrakis, A., Powell, H. R., Read, R. J., Rigden, D. J., Rochira, W., Sammito, M., Sánchez Rodríguez, F., Sheldrick, G. M., Shelley, K. L., Simkovic, F., Simpkin, A. J., Skubak, P., Sobolev, E., Steiner, R. A., Stevenson, K., Tews, I., Thomas, J. M. H., Thorn, A., Valls, J. T., Uski, V., Usón, I., Vagin, A., Velankar, S., Vollmar, M., Walden, H., Waterman, D., Wilson, K. S., Winn, M. D., Winter, G., Wojdyr, M. & Yamashita, K. (2023). *Acta Cryst.* D**79**, 449–461.

Barglow, K. T., Saikatendu, K. S., Bracey, M. H., Huey, R., Morris, G. M., Olson, A. J., Stevens, R. C. & Cravatt, B. F. (2008). *Biochemistry*, **47**, 13514–13523.
Benoit, S. L., Maier, R. J., Sawers, R. G. & Greening, C. (2020). *Microbiol. Mol. Biol. Rev.* **84**, e00092-19.
Bork, P. & Koonin, E. V. (1994). *Protein Sci.* **3**, 1344–1346.
Cederfelt, D., Badgujar, D., Au Musse, A., Lohkamp, B., Danielson, U. H. & Dobritzsch, D. (2023). *Biomolecules*, **13**, 1763.
Chiu, W.-C., You, J.-Y., Liu, J.-S., Hsu, S.-K., Hsu, W.-H., Shih, C.-H., Hwang, J.-K. & Wang, W.-C. (2006). *J. Mol. Biol.* **359**, 741–753.
Collaborative Computational Project, Number 4 (1994). *Acta Cryst.* D**50**, 760–763.
Cover, T. L. & Blaser, M. J. (2009). *Gastroenterology*, **136**, 1863–1873.
Emsley, P. & Cowtan, K. (2004). *Acta Cryst.* D**60**, 2126–2132.
Emsley, P., Lohkamp, B., Scott, W. G. & Cowtan, K. (2010). *Acta Cryst.* D**66**, 486–501.
Gouet, P., Courcelle, E., Stuart, D. I. & Métoz, F. (1999). *Bioinformatics*, **15**, 305–308.
Gouet, P., Robert, X. & Courcelle, E. (2003). *Nucleic Acids Res.* **31**, 3320–3323.
Jin, C., Jin, H., Jeong, B.-C., Cho, D.-H., Chun, H.-S., Kim, W.-K. & Chang, J. H. (2021). *Crystals*, **11**, 499.
Kabsch, W. (2010). *Acta Cryst.* D**66**, 125–132.
Krissinel, E. (2015). *Nucleic Acids Res.* **43**, W314–W319.
Krissinel, E. B., Winn, M. D., Ballard, C. C., Ashton, A. W., Patel, P., Potterton, E. A., McNicholas, S. J., Cowtan, K. D. & Emsley, P. (2004). *Acta Cryst.* D**60**, 2250–2255.
Kuhns, L. G., Benoit, S. L., Bayyareddy, K., Johnson, D., Orlando, R., Evans, A. L., Waldrop, G. L. & Maier, R. J. (2016). *J. Bacteriol.* **198**, 1423–1428.
Liu, H., Gao, Y., Zhang, M., Qiu, X., Cooper, A. J. L., Niu, L. & Teng, M. (2013). *Acta Cryst.* D**69**, 1470–1481.
Lundgren, S., Lohkamp, B., Andersen, B., Piškur, J. & Dobritzsch, D. (2008). *J. Mol. Biol.* **377**, 1544–1559.
Makumire, S., Su, S., Weber, B. W., Woodward, J. D., Wangari Kimani, S., Hunter, R. & Sewell, B. T. (2022). *J. Struct. Biol.* **214**, 107859.
Malfertheiner, P., Camargo, M. C., El-Omar, E., Liou, J. M., Peek, R., Schulz, C., Smith, S. I. & Suerbaum, S. (2023). *Nat. Rev. Dis. Primers*, **9**, 19.
Maurer, D., Lohkamp, B., Krumpel, M., Widersten, M. & Dobritzsch, D. (2018). *Biochem. J.* **475**, 2395–2416.
McCoy, A. J., Grosse-Kunstleve, R. W., Adams, P. D., Winn, M. D., Storoni, L. C. & Read, R. J. (2007). *J. Appl. Cryst.* **40**, 658–674.
Moss, S. F., Chey, W. D., Daniele, P., Pelletier, C., Jacob, R., Tremblay, G., Hubscher, E., Leifke, E. & Malfertheiner, P. (2023). *Ther. Adv. Gastroenterol.* **16**, 17562848231167284.
Nair, A. V., Singh, A. & Chakravortty, D. (2025). *Redox Biol.* **83**, 103648.
Nel, A. J., Tuffin, I. M., Sewell, B. T. & Cowan, D. A. (2011). *Appl. Environ. Microbiol.* **77**, 3696–3702.
Pace, H. C., Hodawadekar, S. C., Draganescu, A., Huang, J., Bieganowski, P., Pekarsky, Y., Croce, C. M. & Brenner, C. (2000). *Curr. Biol.* **10**, 907–917.
Piotrowski, M., Janowitz, T. & Kneifel, H. (2003). *J. Biol. Chem.* **278**, 1708–1712.
Raczynska, J. E., Vorgias, C. E., Antranikian, G. & Rypniewski, W. (2011). *J. Struct. Biol.* **173**, 294–302.
Robert, X. & Gouet, P. (2014). *Nucleic Acids Res.* **42**, W320–W324.
Rodríguez-Hernández, D., Vijayan, K., Zigweid, R., Fenwick, M. K., Sankaran, B., Roobsoong, W., Sattabongkot, J., Glennon, E. K. K., Myler, P. J., Sunnerhagen, P., Staker, B. L., Kaushansky, A. & Grøtli, M. (2023). *Nat. Commun.* **14**, 5408.
Sagar, N. A., Tarafdar, S., Agarwal, S., Tarafdar, A. & Sharma, S. (2021). *Med. Sci.* **9**, 44.
Sakai, N., Tajika, Y., Yao, M., Watanabe, N. & Tanaka, I. (2004). *Proteins*, **57**, 869–873.
Sekula, B., Ruszkowski, M., Malinska, M. & Dauter, Z. (2016). *Front. Plant Sci.* **7**, 350.
Serbzhinskiy, D. A., Clifton, M. C., Sankaran, B., Staker, B. L., Edwards, T. E. & Myler, P. J. (2015). *Acta Cryst.* F**71**, 594–599.
Stacy, R., Begley, D. W., Phan, I., Staker, B. L., Van Voorhis, W. C., Varani, G., Buchko, G. W., Stewart, L. J. & Myler, P. J. (2011). *Acta Cryst.* F**67**, 979–984.
Studier, F. W. (2005). *Protein Expr. Purif.* **41**, 207–234.
Wang, W. C., Hsu, W. H., Chien, F. T. & Chen, C. Y. (2001). *J. Mol. Biol.* **306**, 251–261.
Warren, J. R. & Marshall, B. (1983). *Lancet*, **321**, 1273–1275.
Williams, C. J., Headd, J. J., Moriarty, N. W., Prisant, M. G., Videau, L. L., Deis, L. N., Verma, V., Keedy, D. A., Hintze, B. J., Chen, V. B., Jain, S., Lewis, S. M., Arendall, W. B., Snoeyink, J., Adams, P. D., Lovell, S. C., Richardson, J. S. & Richardson, J. S. (2018). *Protein Sci.* **27**, 293–315.
Winn, M. D., Ballard, C. C., Cowtan, K. D., Dodson, E. J., Emsley, P., Evans, P. R., Keegan, R. M., Krissinel, E. B., Leslie, A. G. W., McCoy, A., McNicholas, S. J., Murshudov, G. N., Pannu, N. S., Potterton, E. A., Powell, H. R., Read, R. J., Vagin, A. & Wilson, K. S. (2011). *Acta Cryst.* D**67**, 235–242.